WALL EFFECTS ON THE EXCITATION AND PROPAGATION OF INSTABILITIES IN HALL THRUSTERS

N. Gascon and M. A. Cappelli
Stanford University, Mechanical Engineering Department, Thermosciences Division
Stanford, CA94305-3032
cap@stanford.edu

ABSTRACT

We present recent experimental results of the use of electrostatic probes to characterize the differences seen in the low frequency instabilities (<200 kHz) in a laboratory Hall discharge operating with two very different wall materials - alumina and boron nitride. A wavelet decomposition analysis of the probe signals was used to determine the dispersion and turbulent broadening characteristics, which have a strong dependence on the axial location within the channel. The azimuthal direction of propagation is shown to be closely linked to the directions of the density and magnetic field gradient drifts. While the general behavior seen with the two wall materials is similar, a noticeable difference is in the location of the ionization zone, as determined by the location in the peak of the plasma density. The location of the ionization zone with alumina walls remains very close to where the magnetic field peaks, whereas with boron nitride walls, they are separated by 20-30 mm. As a result, the direction of the gradient driven electron drift in these two cases differ somewhat, leading to differences in the propagation characteristics of the disturbances. The possible impact that these disturbances in plasma density may have on electron transport properties is discussed.

I. INTRODUCTION

The Hall effect plasma accelerator (also referred to as Hall thruster or Stationary Plasma Thruster) [1-2] is presently the subject of considerable research as it is considered to be the propulsion method of choice for many spacecraft missions. In a typical Hall effect plasma source, a magnetic field is applied perpendicularly to the flow of electrons in the discharge, creating a zone of high resistivity and strong electric field. The strength of the magnetic field is sufficiently low such that it does not directly affect the motion of the more massive ions. The ions react only to the local electrostatic field, which accelerates them to high velocities, typically within 50 % - 70 % of applied discharge voltage. The discharge is sustained between an external cathode and an anode (which also serves as the propellant gas distributor) at the base of an annular dielectric channel. Only a small fraction of the cathode-emitted electrons migrate towards the anode to service the discharge (some 10 %), while most follow the ion plume to neutralize its space charge. Modern versions of these thrusters have an annular discharge chamber of 10-15 cm in diameter, consume about 5-20 mg/s of xenon gas, 1-5 kW of electricity, and produce a thrust in the range of 100-200 mN, with a thrust power to input power ratio in excess of 0.5 (50 % efficiency).

It has been known since the 1960's, when discharges of this type were first studied for use as space propulsion devices, that the electron conductivity is much higher than that predicted by classical theory of cross-field transport [3] – a result not unexpected for plasmas with strongly magnetized electrons, as the classical Hall parameter (ratio of electron cyclotron frequency to electron collision frequency for momentum transfer), $\omega_e/\nu_e \gg 1$. Little is understood about the origin for this anomalous electron flow, despite the fact that it is the critical link between the externally applied magnetic field and the self-consistent electric field that gives the ion stream its shape and energy. Any numerical simulation that attempts to predict the structure of the ensuing ion stream must include a mechanism/model for this anomalous electron transport.

The mechanisms responsible for anomalous electron conductivity in a Hall thruster discharge fall into two categories: (i) electron scattering from fluctuations in the electric field due to plasma instabilities, and (ii) electron interactions with the dielectric wall – the so-called near-wall conductivity [2]. Recent theoretical studies taking into account secondary electron emission from the wall suggested that wall interactions could account for the qualitative discharge behavior (observed current) at high voltages (>200 V for peak magnetic fields of 10^{-2} T), when the ion current has reached a maximum. However, at low discharge voltages, classical and near-wall conductivity do not seem to account for the observed discharge current, and, it is speculated that at least in this regime, the role of plasma instabilities is very likely to be important.

This paper serves to report on our most recent investigations into the turbulent nature of these discharges, with an emphasis on providing detailed insight into the excitation and propagation of instabilities within the annular discharge channel. We show that disturbances in the plasma density propagate in ways that depend, in part, on the shape of the radial magnetic field, B_r, and plasma density, n_e. We also demonstrate that the propagation behavior of these instabilities depend on the type of ceramic dielectric that lines the channel. In this study, we compare, in detail, the dispersion characteristics of instabilities in Hall discharges lined with either alumina (Al_2O_3) or boron nitride (BN) channels.

II. EXPERIMENTS

II.1. Laboratory Hall Discharge

The Hall discharge studied here is a laboratory version of a nominally low-power (<1 kW) Hall thruster, and is described in more detail in previous papers [4-6]. This particular source is intended to be used as a test bed for studying the discharge physics and not as an operational prototype plasma accelerator, although the design is similar to that of thrusters used in practice. It consists of an annular ceramic channel, 90 mm in diameter, 11 mm in width, and 80 mm in length. A magnetic field driven by four outer coils, one inner coil, and three iron plates provide a magnetic field (mostly radial in direction) peaked 5 mm upstream of the exit of the discharge channel.
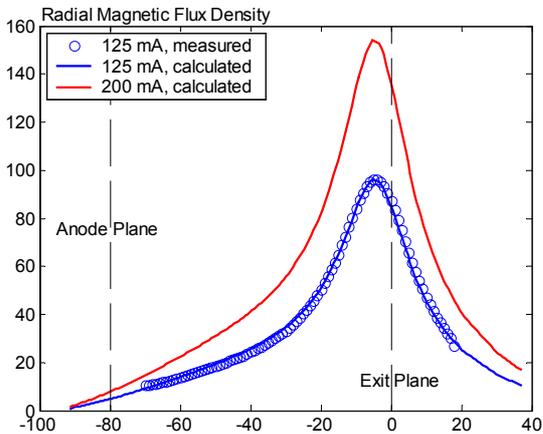

Fig. 2. Axial variation in the magnetic field distribution (radial component) mid-way between the inner and outer wall.

Details of the two-dimensional magnetic field distribution for various magnet currents can be found in Ref. [5]. Figure 2 shows the axial variation in the radial component of the magnetic field at the mean radius of the channel, as computed with a 2-D axisymetric finite-element model, for two values (125 mA and 200 mA) of the magnetic coil current. Experimental measurements of the magnetic field distribution indicate that the radial component of the magnetic field drops off by approximately 15 % at the inner and outer walls of the acceleration channel. A hollow stainless steel ring with 32 holes of 0.5 mm diameter serves both as the anode and the propellant (gas) input of the discharge. A commercial hollow cathode (Ion Tech HCN-252) is used to neutralize the resulting ion beam and provide the necessary electron current to s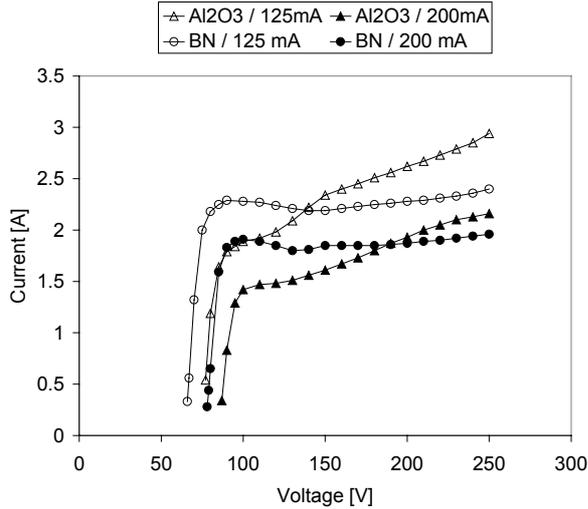ustain the discharge. The cathode is mounted such that its exit aperture is approximately 2 cm downstream of the channel (either the Al_2O_3 or BN) exit.

II.2. Vacuum chamber

All experiments reported here were performed in a 1 m diameter by 1.5 m long stainless steel vacuum chamber. Flanged elbows (0.5 m in diameter) at each end of the vacuum chamber supported two 0.5 m diameter diffusion pumps, operated without baffles for maximum pumping speed (approximately 6000 l/s). This pumping plant provided an operating pressure of 10^{-4} torr, as indicated by an ionization gauge (uncorrected for xenon). Separate direct-current (DC) power supplies powered the anode, cathode heater, cathode keeper, and magnet coils. For the measurements reported on here, the xenon flow rate at the anode was 2 mg/s. An additional 0.3 mg/s of xenon flow was necessary for running the hollow cathode, the body of which was kept at vacuum chamber ground potential. The discharge voltage and current were monitored with digital multimeters. Discharge current oscillations were measured with a powered differential amplifier (Tektronix P5200) placed across a 4 Ω series resistor and recorded by a high-speed PC-based 4-channel digital oscilloscope (National Instruments PCI-5102), with a 20 MHz maximum sampling rate and 12-bit maximum vertical resolution.

Fig. 3. Current-voltage characteristics of the laboratory Hall discharge studied.

II. 3. Discharge characterization

Current-voltage (I-V) characteristics of the thruster operating with both BN and Al_2O_3 walls are shown in Fig. 3. With Al_2O_3 walls, the discharge current increases continuously with applied voltage, whereas with BN walls, the I-V curve is more characteristic of that of modern Hall thrusters, first increasing rapidly ("ionization branch"), then decreasing between 100 V-150 V, only to plateau (or increase slightly) between 150 V and 200 V (so called "current saturation" branch). In the ionization branch, the rapid increase in discharge current with increased voltage is due to the increased mean electron energy, resulting in a higher ionization rate and higher ionization fraction (avalanche ionization). At higher voltage, the ionization fraction has reached a maximum value (nearly 100% propellant utilization, *i.e.*, the conversion of neutral xenon to ionized xenon), and the discharge current either remains constant or increases slightly due to changes in electron mobility. At present, there is no satisfactory explanation given so far in the Hall thruster literature about the appearance of the negative resistance region in the I-V curve, located here at approximately 100V for the discharge with BN walls, even though it seems to be a general feature of modern Hall thruster behavior.

The difference in the I-V characteristics for the two wall materials suggests that plasma - wall interactions play an important role in the sustaining of this discharge. Since the earliest near-wall conductivity theory proposed by Morozov in the 1960s [7], it has been widely accepted that the secondary electron emission property of the wall material has a significant influence in the discharge behavior. The secondary electron process is involved through two effects: (i) wall materials with high γ_{se} give rise to high cross-field electron conductivity (wall conductivity), since a large fraction of the incident electrons are returned to the plasma with a new guiding center drift along the direction of the electric field; (ii) the secondary electrons have energies that are, on average, lower than the primaries, resulting in a cooling of the discharge, a lower ion production rate and therefore, a lower ion current. Based on recent numerical simulations on a similar discharge to that studied here [8], it appears that the first effect is predominant at high discharge voltages, where the electron energy losses to the wall are limited by the space charge-saturation of the sheath, whereas the second effect dominates in the ionization regime of the discharge. This is consistent with the results shown in Fig. 2, since over the range of electron energies expected, $\gamma_{se}(Al_2O_3) > \gamma_{se}(BN)$.

It is noteworthy that the discharge current is not at all "steady" in these Hall thrusters, but rather, exhibits fluctuations coincident with instabilities in the plasma properties [9]. A detailed study of the discharge current oscillations seen in this thruster was presented in a previous paper [10]. Below, we describe a detailed study of intrinsic plasma density disturbances that are excited and propagate within the discharge channel, as detected using Langmuir probes.

II.4. Langmuir probes

Plasma density fluctuations inside the channel and near the exit plane were characterized by three azimuthally placed low-impedance Langmuir probes biased negatively with respect to the plasma potential to collect the ion saturation current. For isothermal fluctuations, the collected current measures fluctuations in the local ion density. The exposed part of the probes consisted of a 0.254 mm diameter, 5 mm long tungsten wire. The remaining body of the probe is made of an alumina tube directly surrounding the tungsten wire (0.508 mm ID, 1.27 mm OD), followed by a stainless steel tube (1.48 mm ID, 1.58 mm OD), connected to the braided ground of a 50 Ω co-axial cable. The inner tungsten wire was connected to the center pin of the co-axial cable. This outer stainless steel tubing served as a Faraday shield to isolate the extended probe base from disturbances other than those at the tip of the probe. The stainless steel tubing was then surrounded by another alumina tube (1.6 mm ID, 2.3 mm OD) and the entire inside air spaces were potted with an alumina paste.

The probe body length (10 cm) was minimized so as to reduce its overall capacitance. The frequency response of the probe was found to be excellent (unity gain and no measurable phase shift within the measuring device accuracy) up to 1 MHz, with a 3 dB cutoff at 4 MHz. A coaxial transmission line feed-through provided the transfer of the probe signal through the vacuum chamber to the 4-channel digital oscilloscope card operating at a 1 MHz sample rate for the measurement reported on here. The recorded signals were 100,000 samples long. The probes were terminated with 50 Ω at the input of the oscilloscope card. In this way, the probe tips were negatively biased (close to system ground) with respect to the plasma, which is predominantly at high positive potential, since the anode is maintained at a minimum of 83 V, and since the near exit plane potential is always greater than 40 V due to the cathode fall and finite electron temperature.

The orientation of the probes and their relative location and positioning within the thruster are shown in Fig. 4. The triangular configuration was chosen for capturing both the axial and azimuthal components of the wavevectors corresponding to propagating plasma instabilities. The exposed parts of the probes were bent and aligned to be parallel to the radial coordinate in order to prevent shadowing effects. For such an orientation, there is a directed energy flux in addition to the Bohm flux, and so a quantitative interpretation of the magnitude of the signal would require a probe theory accounting for the directed ion energy flux on the front surface of the probe. However, a comparison to prior measurements taken with axially-oriented probes [11] confirms that the results are not very sensitive to probe orientation, and that current collection is still in the ion saturation regime.
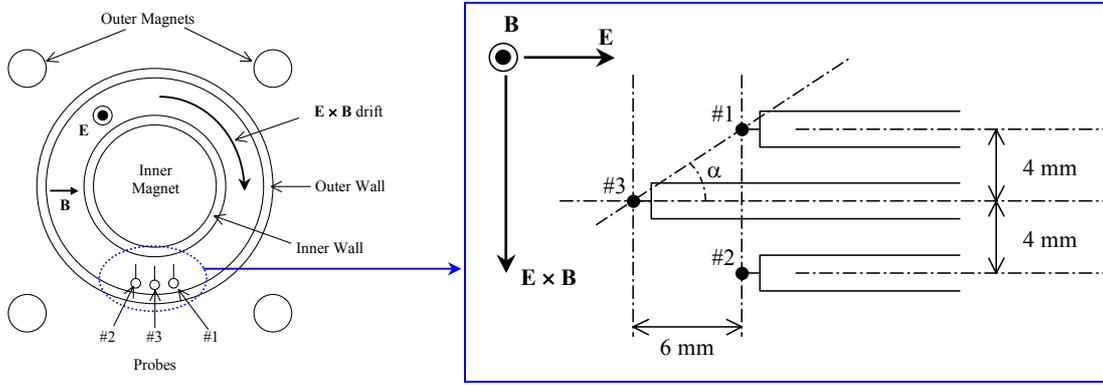

Fig. 4. Schematic of probe locations and orientation.

Probe translation along the axial direction was provided by a translation stage driven by a Slo-Syn stepper motor, powered and controlled by a Compumotor model SX Microstepping Drive/Indexer System. For this study, the axial locations of probe #1 and #2 varied between a distance of approximately 60 mm from the anode (z = - 60 mm) and 30 mm beyond the exit plane (z = 30 mm), with the z = 0 reference taken to be the exit plane of the discharge, and negative positions implying that the probe locations are inside the discharge channel. For any given position z, the location of probe #3 was z - 6 mm.

III. RESULTS AND DISCUSSION

III.1. Joint frequency-wavenumber spectrum

We determine the propagation characteristics of the plasma density fluctuations [12,13] by building a two-dimensional wave dispersion (frequency vs. wavenumber) histogram of the fluctuation power. The recorded signals $S(\mathbf{x},t)$ are decomposed on a base of complex Morlet wavelets:

$$\tilde{S}(\mathbf{x},a,\tau) = \int S(\mathbf{x},t) \frac{1}{\sqrt{a}} h^*(\frac{t-\tau}{a}) \, dt \ ,$$

where:

$$h(t) = \pi^{-1/4} \exp(-\frac{t^2}{2}) \exp(2\pi i t)$$

The scale a of the analyzing wavelets is the inverse of the chosen frequency f in the histogram. For every pair of coefficients ($\tilde{S}(\mathbf{x}_1, a, \tau), \tilde{S}(\mathbf{x}_2, a, \tau)$), the estimated angular wavenumber $2\pi k_{12}$ is the phaseshift (*i.e.* the phase of the cross-power $\tilde{S}^*(\mathbf{x}_1, a, \tau)\tilde{S}(\mathbf{x}_2, a, \tau)$) divided by the probe separation distance $|\mathbf{x}_2 - \mathbf{x}_1|$, and the contribution to the histogram P_{12}^2 is taken as the mean amplitude:

$$P_{12}^2 = \frac{1}{2}\left(\tilde{S}^*(\mathbf{x}_1, a, \tau)\tilde{S}(\mathbf{x}_1, a, \tau) + \tilde{S}^*(\mathbf{x}_2, a, \tau)\tilde{S}(\mathbf{x}_2, a, \tau) \right)$$

Using wavelet decomposition and time average instead of the classical Fourier decomposition and ensemble average results in greater statistical robustness of the estimated dispersion characteristics and allows resolving transients and soliton-like features [13]. This method also allows estimating the second moment of the spectrum, the wavenumber "spectral width", analogous to the "kurtosis", which can be viewed as a measure of the turbulent broadening of the dispersion relation [12].

The wavenumbers extracted from the pair of signals are projections of the propagation wavevectors on the probe pair vector:

$$k_{12} = \mathbf{k} \cdot (\mathbf{x}_2 - \mathbf{x}_1)\frac{1}{|\mathbf{x}_2 - \mathbf{x}_1|}$$

However, with a three-probe arrangement, it is possible to determine both the azimuthal and longitudinal components of the wavevectors by analysis of the signal on any two different pairs of probes. With our particular arrangement, for every component in the wavelet decomposition, we have for example:

$$k_z = \frac{\sqrt{13}}{6}(k_{31} + k_{32}) \;;\; k_\theta = \frac{\sqrt{13}}{4}(k_{32} - k_{31}) \;;\; P_z^2 = \frac{9}{13}(P_{31} + P_{32})^2 \;;\; P_\theta^2 = \frac{4}{13}(P_{32} - P_{31})^2$$

We verified that a k_θ analysis with all 3 probes gives similar results as a k_{12} analysis with only probes #1 and #2, since these are located purely along the azimuthal direction.
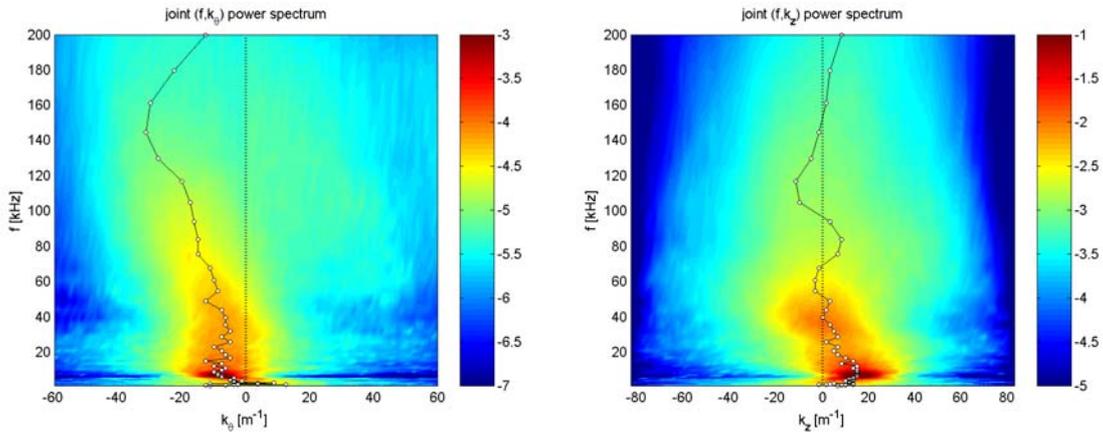

Fig. 5. Examples of dispersion maps and the dispersion curves for the strongest mode. This case is for the discharge operating with an Al_2O_3 channel and probes near the region of the peak in the magnetic field. The applied discharge voltage $U_d = 100$ V and the coil current $I_B = 125$ mA.

Figure 5 provides an example of a typical dispersion map ("joint power spectrum") resulting from this analysis when probes #1 and #2 are at an axial position of 5 mm upstream of the channel exit (near the peak of magnetic field) and probe #3 is located at an axial position of 11 mm upstream of the exit. The dispersion relation of the strongest mode (*i.e.* the wavenumber of the disturbance contributing the greatest power, as a function of frequency) is indicated with a black line. It is apparent, that at this location, the disturbances generally propagate in the direction opposite the electron drift (negative k_θ), and towards the cathode (positive k_z) at low frequencies. It is apparent then, that at this location, the low-frequency (<60 kHz) disturbances are tilted azimuthal waves, in particular, the strongest mode at about 10 kHz, with wavelengths

corresponding to approximately $1/3^{rd}$ -$1/4^{th}$ of the channel circumference, i.e., with mode numbers between m = 3 - 4. The phase velocity of these low frequency disturbances is ~3×10^3 m/s.

The corresponding turbulent broadenings (from the wavenumber spectral width) of the disturbances are shown in Fig. 6. Only the regions where the number of events is above average are shown, for statistical significance. The dispersion relation of the strongest mode is again superimposed on the plots.
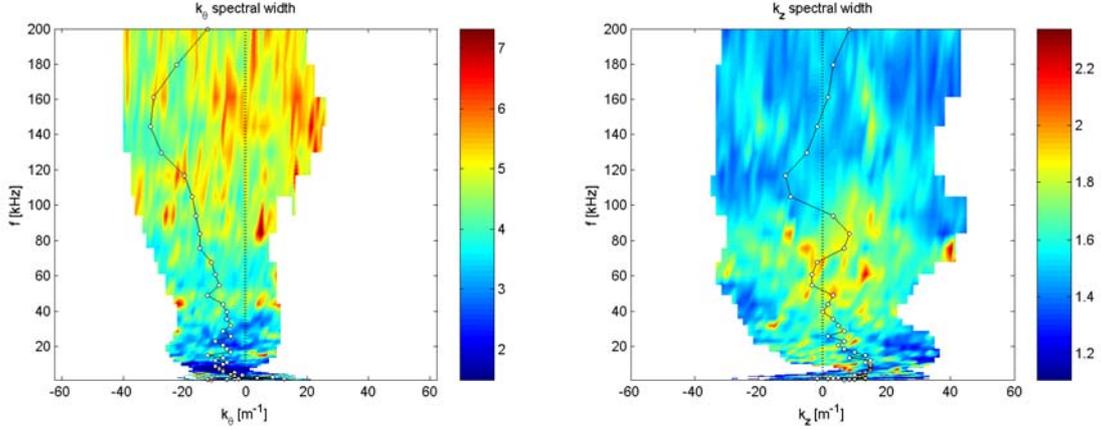

Fig. 6. Examples of wavenumber spectral width (turbulent broadening), and dispersion relation of the strongest mode. The experimental parameters are the same as those in Fig. 5.

From Fig. 5 and 6, it can be seen that the strongest fluctuations (frequencies below 30 kHz) have relatively low spectral widths, indicating that these very low frequency disturbances are very coherent. Between 30 kHz and 80 kHz, there is a region of fairly strong, mostly azimuthal (k_θ = 10-20 m^{-1}, k_z = 0 m^{-1}) fluctuations that are somewhat coherent in the azimuthal direction, but appear to be rather turbulent in the axial direction of propagation. At higher frequencies (>80 kHz), the propagation is still largely along the azimuthal direction, with k_θ increasing to as high as 40 m^{-1}, however, the broadening now appears along the azimuthal direction, with rather coherent fluctuations along the axial direction.

III. 2. Plasma density fluctuation maps

In order to compare the effect that the channel wall material has on discharge behavior, the operating parameters were constrained to an applied voltage of 110 V and an electromagnet current of 200 mA. This operating point is located on the "knee" of the current-voltage characteristics of the discharge (see Fig. 3), in the vicinity of the negative resistance region with a BN channel. In this region of the I-V curve, we believe that there must be some anomalous electron conductivity due to fluctuations, since at higher voltages, as the total current decreases, the ion current *increases* as does the electron temperature (and hence wall conductivity). As discussed above, the lower current for the case of Al$_2$O$_3$ walls, in this region, is likely due to the lower electron temperature (because of its higher γ_{se}), and hence lower degree of ionization.

Figure 7 plots the spatial and frequency-dependence (k_θ on the left, where positive values are along the direction of the **E**×**B** drift, except in the lower pane, where the direction of **B** is reversed, k_z on the right panels, where positive values are directed towards the cathode) of the component wavenumbers of the strongest modes, n_e, and B_r. Figure 8 plots the corresponding power spectral maps (left panels) and propagation angle of the strongest mode (right panels), as well as the amplitude in the plasma density fluctuations (circles in the left panels) and the local inhomogeneity parameter, L_∇, defined by [14]:

$$L_\nabla^{-1} = \frac{B_r}{n_e}\frac{\partial}{\partial z}\left(\frac{n_e}{B_r}\right)$$

This parameter was first introduced as it pertains to Hall discharges for characterizing the growth and propagation of the so-called "spoke" instability [3].

The first noticeable wall related effect is the difference in the position of the peak plasma density, as seen in the first two panels on the left side of Fig. 7. For the case of Al$_2$O$_3$ walls, the peak in n_e is located about 15 mm upstream of the channel exit, whereas with BN walls, it is a further 15 mm towards the anode (30 mm from the exit). Though not shown in the figure, we have found [10] that with BN walls, the peak

tends to move even further towards the anode at higher voltages (150 V), and towards the exit at lower voltage (83 V). The shifts towards the anode are accompanied by a narrowing of the spatial distribution. Similar behavior, although not as pronounced, was seen with the Al_2O_3 walls [6]. This shift in n_e can be understood qualitatively by recognizing that the plasma density is established through a balance between ionization and ion acceleration. Moving from the anode towards the cathode, the rise in density reflects an increased ionization (expected to be greater for the case of BN, because of the higher T_e, all else equal), while the subsequent fall in plasma density reflects the acceleration (which is delayed in the case of Al_2O_3, because of the lower fraction ion current). It is noteworthy that the change in wall material does not seem to have any significant effect on the location of the secondary plasma density peak at z = -40 mm.
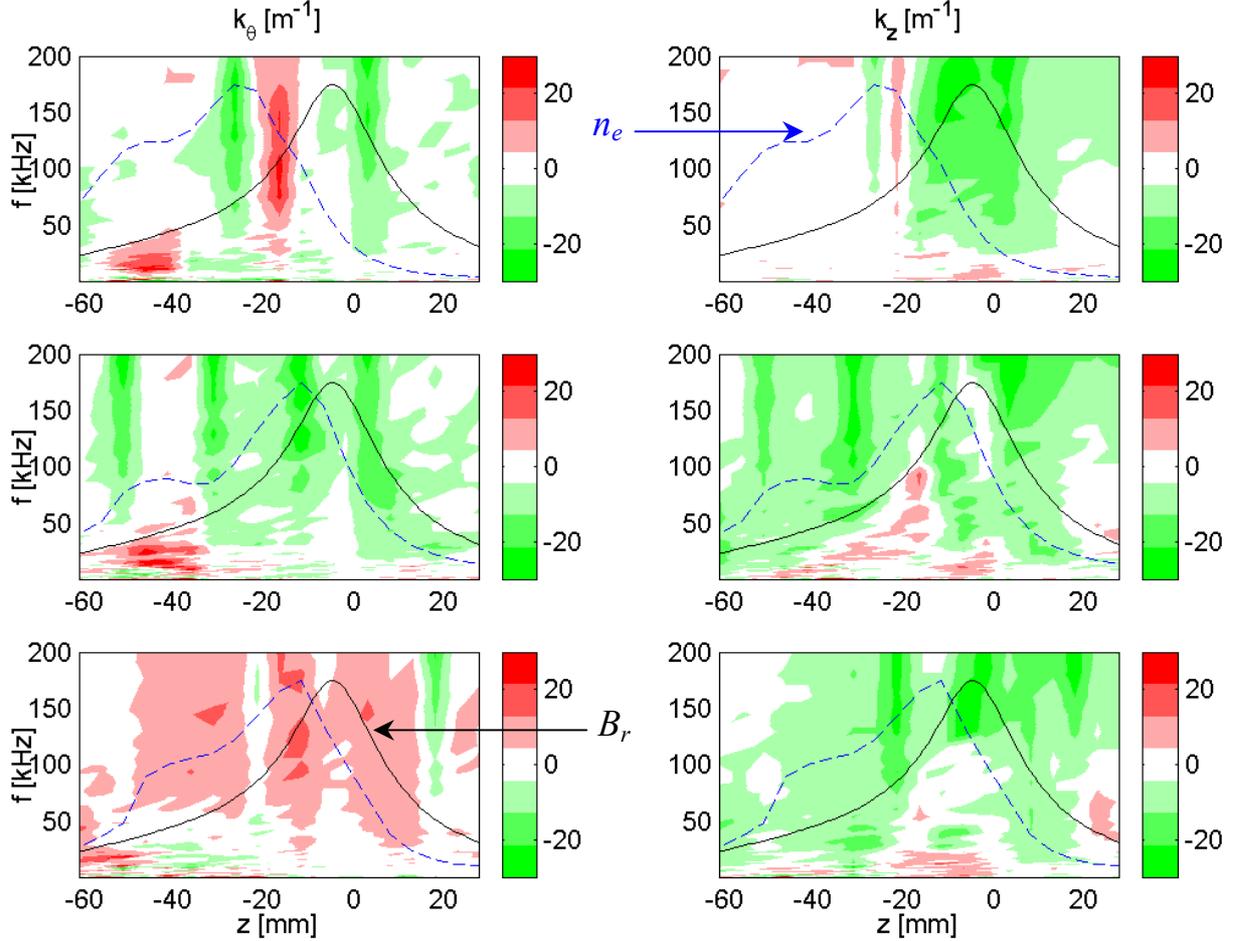

Fig. 7: Dispersion relation maps and longitudinal profiles of the plasma density and radial magnetic field. The exit plane is located at z = 0. U_d = 110 V ; I_B = 200 mA. Top: BN walls. Middle and Bottom: Al_2O_3 walls. Top and Middle: radial magnetic field oriented inwards. Bottom: radial magnetic field oriented outwards.

As indicated by the curves in the left panels of Fig. 8, the amplitude of the plasma density fluctuations follows (qualitatively) the spatial variation in the mean shown in Fig. 7. The frequency spectrum of these fluctuations (the maps in the left panels of Fig. 8) depicts features common to both the BN and Al_2O_3 wall cases. The strongest features are concentrated in a narrow peak near 10 kHz, spread throughout the channel, and are attributed to the so-called "breathing mode" [15]. There is a distribution of broader disturbances ranging from 20-200 kHz (and beyond) throughout the channel. Note that these spectral maps have been normalized by the total power in the fluctuations at any given axial location.

With reference to Fig. 7, we see features (peaks and inflections) in the axial profile of n_e, and B_r that coincide with the azimuthal and axial propagation characteristics of the strongest modes. For example, the high frequency (>50 kHz), predominantly azimuthal modes that appear as vertical bands extending to the limit of the frequencies studied (200 kHz) have directions which correlate with directions associated with the combined influence of the density and magnetic gradient drifts on the electron fluid, *i.e.*,

$$\mathbf{v}_{\nabla n} \approx -\frac{\kappa T_e}{2en_e B^2}\nabla n_e \times \mathbf{B} \qquad\qquad \mathbf{v}_{\nabla B} \approx \frac{\kappa T_e}{2eB^3}\nabla B \times \mathbf{B}$$

Here κ is the Boltzmann constant and e the elementary charge. For the case of BN walls, as an example, between axial positions of $z = +10$ mm and $z = 0$ mm, the gradient in the magnetic field is negative, implying a strong magnetic gradient drift along the azimuth, opposite the $\mathbf{E}\times\mathbf{B}$ direction. In this same region, the density profile also has a negative slope (though not as strong as the gradient in B_r), that would drive a density gradient drift in the $\mathbf{E}\times\mathbf{B}$ direction. The favoring of instabilities along the direction opposite the $\mathbf{E}\times\mathbf{B}$ direction is consistent with the relative inhomogeniety measured in this region. Between $z = 0$ mm and $z = -10$ mm, there is no favored azimuth direction in the propagation of the strongest disturbances, most likely because of the canceling out of these gradient drifts. Between $z = -10$ mm and $z = -20$ mm, both the magnetic and density gradient drift velocities are in the $\mathbf{E}\times\mathbf{B}$ direction and the disturbances are seen to propagate predominately in the $\mathbf{E}\times\mathbf{B}$ direction, as evidenced by the small axial component wavenumber as seen in the right panel of the figure. It is noteworthy that this strong disturbance that propagates in the $\mathbf{E}\times\mathbf{B}$ direction is not observed in the case of Al_2O_3 (middle left pane), because of the nearly overlapping density and magnetic field profiles. Just beyond $z = -20$ mm, the propagation direction is again opposite the $\mathbf{E}\times\mathbf{B}$ direction, driven largely by the gradient in the density field. Surprisingly, the direction of propagation (maps in the right panel of Fig. 8) and amplitude of the disturbances (curves in the left panel of Fig. 8) only mildly track the local inhomogeneity parameter, which is also plotted as a line in the right panel of Fig. 8.
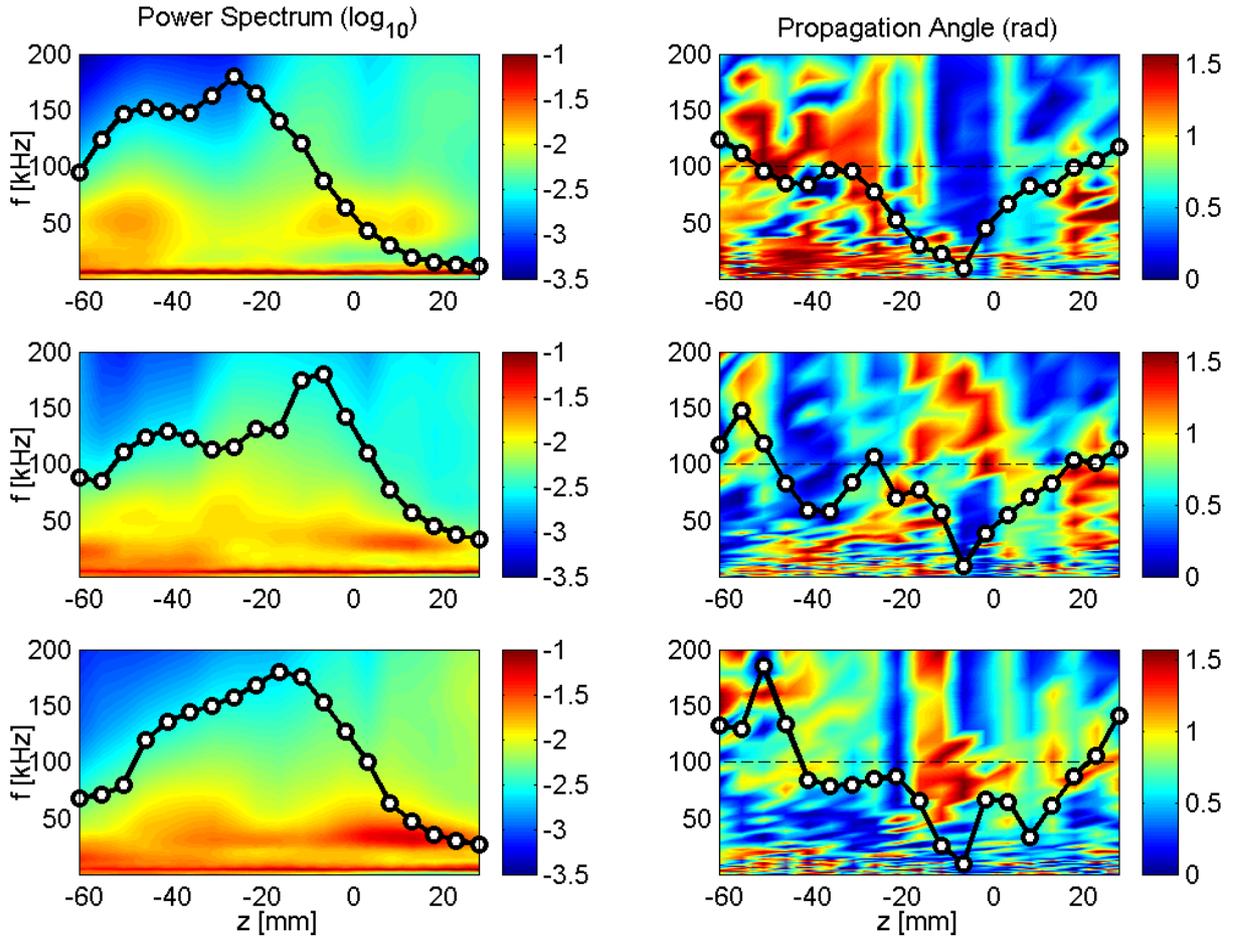

Fig. 8. Left: Frequency spectral maps. Experimental conditions are the same as in Fig. 7. For every position, the spectrum is normalized to the total power (circles). Right: Propagation angle of the strongest mode, and local inhomogeneity parameter L_∇^{-1} (circles; above the dashed line means positive value). A propagation angle of zero (in radians) indicates a purely axial mode, and $\pi/2$ a purely azimuthal mode.

The bottom two (left and right panels) of Fig 7 show that reversing the magnetic polarity does have an effect on the strength and direction of propagation of these disturbances. It is apparent that the propagation characteristics along the azimuthal direction reverse, whereas the characteristics along the axial direction are largely unchanged. This result provides support for the case that these disturbances are gradient-driven, deriving their energy from the work done by forces on the electron fluid by the gradients in field property. It is important to note, however, that reversing the field did alter the shape of the secondary plasma peak near $z = -40$ mm. With the field configuration giving rise to the properties in the middle panel, there are competing gradients which may tend to cancel, hence no favoring in azimuthal direction, whereas with the reversed field, the gradients are always aligned in this region, giving rise to a favored direction opposite that of the **E×B** drift.

It seems that, with the exception of a small region near the peak density in the BN channel, the axial component wavenumbers of disturbances at high frequencies (>50 kHz) are almost always directed towards the anode, in the net direction of electron migration. There are regions of the plasma, within the ionization zone, where low frequency disturbances propagate towards the cathode. These seem to be stronger in the case of Al_2O_3 walls. The velocity of these instabilities are ~10 km/s, which is very close to the ion velocity, making it tempting to assign these to the so-called "transit-time" [1,2,9], as these instabilities have little or no azimuthal component to their direction of propagation.

As discussed in the early Hall discharge literature [3,14,16,17], the low-frequency (<200 kHz) disturbances studied here are believed to contribute to anomalous electron conductivity. While an estimate of the axial electron current, either measured directly [6], or through the measurement of correlated azimuthal electric field fluctuations [3] has not been carried out in this study, we can estimate the effect that these fluctuations have on electron transport, from the statistical theories relating the turbulence intensity of the plasma density fluctuations to the cross-field mobility [18]. We find that for the relatively low voltages studied here, the Hall parameters are approximately 100, which are somewhat larger than the levels expected for Bohm conductivity (~16), yet somewhat below those expected based on classical molecular scattering (~500-1000, see Ref. [6]). The spatial variation in the inverse Hall parameters derived from the turbulence intensities do show a noticeable drop near the region of strong magnetic field, in agreement with previous, more direct measurements of the Hall parameter, on this same discharge [6]. The reason for the drop in the turbulence intensity is still the subject of ongoing research, and is speculated to be attributed to the strong axial variation in the azimuthal electron velocity [19].

IV. SUMMARY

Electrostatic probes were used to characterize low frequency instabilities in a laboratory Hall discharge operating with alumina and boron nitride. A wavelet decomposition analysis of these probe signals was used to determine the dispersion characteristics, which have a strong dependence on the axial location within the channel. The strongest disturbances appear to be excited by the gradient driven azimuthal drifts in the electron flow, over the frequency range of 50 – 200 kHz. The correlation in both the direction of propagation and the strength of the fluctuations seem to only mildly track the sign and magnitude of the local inhomogeneity parameter. It is noteworthy that the turbulence seems to be highly anisotropic. Near the peak in plasma density (where fluctuations are strongest) there is a significant turbulent broadening predominantly in the azimuthal direction at higher frequencies (>80 kHz), predominantly in the axial direction at lower frequencies (20-50 kHz), and very little broadening at low frequencies (10 - 20 kHz), where the disturbances are of large scale (m = 3 or 4), and very coherent.

While the general behavior seen with the two wall materials is similar, a noticeable difference is in the location of the ionization zone, as determined by the location in the peak of the plasma density. The location of the ionization zone with alumina walls remains very close to where the magnetic field peaks, whereas with boron nitride walls, they are separated by 20-30 mm. As a result, the direction of the gradient driven electron drift in these two cases differ somewhat, leading to differences in the propagation characteristics of the disturbances. While this suggests that the differing wall properties may have an indirect effect on the development of instabilities, it is still unclear as to whether there are direct mechanisms by which the interaction of the wall with the plasma enhance or suppress the growth of these instabilities. Theoretical and experimental studies to address this question are the subject of future papers.

ACKNOWLEDGEMENTS

REFERENCES

[1] V.V.Zhurin, H.R. Kaufman, "Physics of closed drift thrusters" *Plasma Sources Sci. Technolo.* 8, R1-R20 (1999)

[2] A.I. Morozov and V.V. Savelyev, "Fundamentals of Stationary Plasma Thruster Theory"*, Reviews of Plasma Physics, 21, pp 203-391,* Consultant Bureau, New York (2000)

[3] G.S. Janes and R.S. Lowder, "Anomalous electron diffusion and ion acceleration in a low-density plasma"*, Phys. Fluids 9, 1115-1123* (1966)

[4] M.A. Cappelli, W.A. Hargus, Jr., and N.B. Meezan, "Coherent structures in crossed-field closed-drift Hall thrusters," *IEEE Trans. Plasma Sciences 27, pp. 96-97* (1999)

[5] W.A. Hargus, Jr., "Investigation of the plasma acceleration mechanism within a co-axial Hall thruster." *Ph.D. Thesis,* Mechanical Engineering Department, Stanford University. (2001).

[6] N.B. Meezan and M.A. Cappelli, "Anomalous Electron Mobility in a Coaxial Hall Discharge," *Phys. Rev. E 63, 026410-1* (2001).

[7] A.I. Morozov, *Zh. Prikl. Mekh. Tekh. Fiz. (in Russian), 3,19* (1968)

[8] S. Barral, K. Makowski, Z. Peradzynski, N. Gascon, and M. Dudeck "Wall material effects in stationary plasma thrusters, part II: Wall conductivity theory", *Submitted to Phys. Plasmas.*

[9] E.Y. Choueiri, "Plasma oscillations in Hall thrusters", *Phys. Plasmas, 8, 4,* (2001)

[10] N. Gascon, N.B. Meezan and Mark A. Cappelli, "Low Frequency Plasma Wave Dispersion and Propagation in Hall Thrusters", *27th International Electric Propulsion Conference, Pasadena, California, IEPC 01-56* (2001)

[11] Enrico Chesta, Cheryl M. Lam, Nathan B. Meezan, Daniel P. Schmidt, and Mark A. Cappelli, "A Characterization of Plasma Fluctuations within a Hall Discharge", *IEEE Trans. Plasma Sciences, 29, 4, pp. 582-591,* (2001)

[12] J.M. Beall, Y.C. Kim and E.J. Powers, "Estimation of the wavenumber and frequency spectra using fixed probe pairs, *J. Appl. Phys. 53, 6* (1982)

[13] T. Dudok de Wit *et al.,* "Determination of dispersion relations in quasi-stationary plasma turbulence using dual satellite data", *Geophysical Research Letters, Vol. 22, No. 19, pp. 2653-2656,* (1995)

[14] A.I. Morozov, Y.V. Esipchuk, A.M. Kapulkin, V.A. Nevrovskii, and V.A. Smirnov, "Effect of the magnetic field on a closed-electron-drift accelerator", *Sov. Phys. – Tech. Phys. 17, pp. 482-487* (1972)

[15] J.-P. Boeuf, L. Garrigues, "Low Frequency Oscillations in a Stationary Plasma Thruster", *Journal of Applied Physics, 84, No. 7, p 3541-3554* (1998).

[16] Y.V. Esipchuk, A.I. Morozov, G.N. Tilinin, A.V. Trofimov, "Plasma oscillations in closed-drift accelerators with an extended acceleration zone", *Sov. Phys. – Tech. Phys. 43, pp. 1466-1473* (1973)

[17] Y.V. Esipchuk and G.N. Tilinin, "Drift instability in a Hall-current plasma accelerator", *Sov. Phys. – Tech. Phys. 21, pp. 417-423* (1976)

[18] S. Yoshikawa and D.J. Rose, "Anomalous Diffusion of a Plasma across a Magnetic Field", *Phys. Fluids, 5, 3, pp. 334-340* (1962)

[19] M.A. Cappelli, N.B. Meezan and N. Gascon, "Transport Physics in Hall Thrusters", *40th AIAA Aerospace and Sciences Meeting and Exhibit, Reno, Nevada, AIAA-2002-0485* (2002)